Int. J. Solids Structures, 1967, Vol. 3, pp. 1031 to 1051. Pergamon Press Ltd. Printed in Great Britain

DYNAMICS OF AN ELASTIC SATELLITE—III*

T. R. ROBE

Department of Engineering Mechanics, University of Kentucky, Kentucky

and

T. R. KANE

Division of Engineering Mechanics, Stanford University, California

5. APPLICATIONS

Several specific cases are discussed in this part in order to demonstrate effects of elasticity on vehicle motion, to illustrate what is meant by the phrases "attitude instability" and "deformation instability," to confirm that gravitational effects on a rotating elastic satellite can be negligible, and to point out that vehicle stability may be sensitive to dimension and spin rate changes. In each example, the instability inequalities are used to make a stability judgment, and these predictions are then checked by numerical integration of the full, nonlinear differential equations.

To indicate the variety of structural arrangements accommodated by the stability analysis developed previously, we consider two basic schemes. The first, intended to focus attention on basic effects of elasticity and on different types of instability, consists of a simple elastic shaft connecting two rigid blocks. The second arrangement, which is considerably more elaborate, involves a truss connecting two cylindrically shaped bodies, and thus simulates a space station. Actual dimensions are specified in both cases in order to make the examples as meaningful as possible; however, once the dimensionless parameters $\delta_1, \ldots, \delta_{10}$ have been calculated, each example may be regarded as representing a large class of problems.

Stiffness matrices for shaft and truss

As a preliminary step, we establish the stiffness matrices for the two connecting structures and show that both meet the restrictions specified in the instability analysis.

Figures 10 and 11 illustrate the two connections under consideration. In both figures, the center point F of the end of the structure adjacent to R_1 is located with respect to the origin of coordinate system X_j^1 by the position vector $\mathbf{f}$ defined as

$$\mathbf{f} = f_1\mathbf{a}_1 + f_2\mathbf{b}_1 + f_3\mathbf{c}_1 \tag{5.1}$$

Because the stiffness matrix $[S]$ is to be referred to the mass center P_1 for coordinate system X_j^1, the stiffness matrix $[s]$ with respect to point F for coordinate axes X_j^1 will be computed

* Parts I and II of this paper appeared in previous issues of this journal (vol. 3, pp. 333–352 and 691–703, respectively).

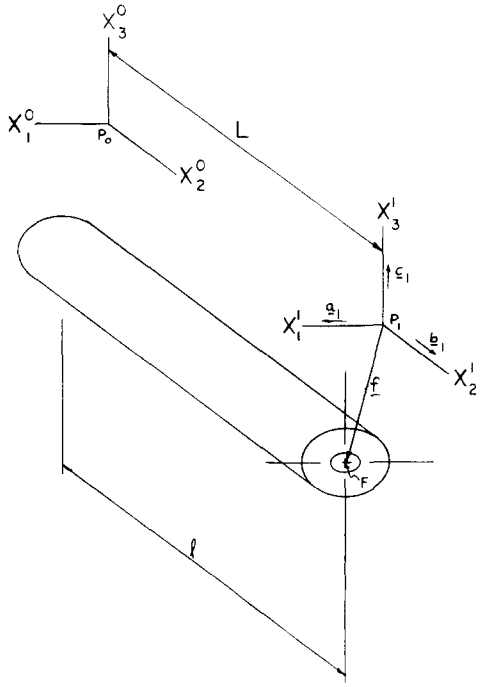

FIG. 10. Shaft.

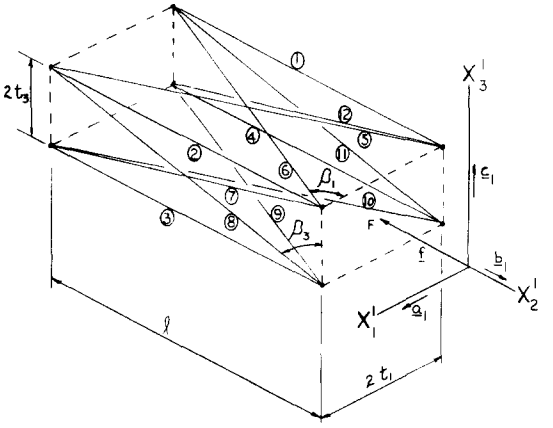

FIG. 11. Truss.

and then transformed to point P_1 by the relationship*

$$[S] = [t]^T[s][t] \tag{5.2}$$

where

$$[t] = \begin{bmatrix} 1 & 0 & 0 & 0 & f_3 & -f_2 \\ 0 & 1 & 0 & -f_3 & 0 & f_1 \\ 0 & 0 & 1 & f_2 & -f_1 & 0 \\ 0 & 0 & 0 & 1 & 0 & 0 \\ 0 & 0 & 0 & 0 & 1 & 0 \\ 0 & 0 & 0 & 0 & 0 & 1 \end{bmatrix} \tag{5.3}$$

and $[t]^T$ is the transpose of $[t]$. As the form of $[s]$ for both the shaft and the truss proves to be

$$[s] = \begin{bmatrix} s_{11} & 0 & 0 & 0 & 0 & s_{16} \\ 0 & s_{22} & 0 & 0 & 0 & 0 \\ 0 & 0 & s_{33} & s_{34} & 0 & 0 \\ 0 & 0 & s_{43} & s_{44} & 0 & 0 \\ 0 & 0 & 0 & 0 & s_{55} & 0 \\ s_{61} & 0 & 0 & 0 & 0 & s_{66} \end{bmatrix} \tag{5.4}$$

* This topic is discussed fully in a forthcoming publication *Dynamics of Elastically Connected Rigid Bodies* by W. Weaver, Jr. See *Developments in Theoretical and Applied Mechanics*, edited by W. A. SHAW. Pergamon Press.

it follows from equation (5.2) that $[S]$ can have a form compatible with the restrictions (4.15) only if f_1 and f_3 are zero, i.e. if the center line of the undeformed structure coincides with the axes X_2^i. $[S]$ is then given by

$$[S] = \begin{bmatrix} s_{11} & 0 & 0 & 0 & 0 & -f_2 s_{11} + s_{16} \\ 0 & s_{22} & 0 & 0 & 0 & 0 \\ 0 & 0 & s_{33} & f_2 s_{33} + s_{34} & 0 & 0 \\ 0 & 0 & f_2 s_{33} + s_{43} & s_{44} & 0 & 0 \\ 0 & 0 & 0 & 0 & s_{55} & 0 \\ -f_2 s_{11} + s_{61} & 0 & 0 & 0 & 0 & f_2^2 s_{11} - 2 f_2 s_{16} + s_{66} \end{bmatrix} \tag{5.5}$$

For the circular shaft, the stiffness matrix* elements are

$$\left.\begin{aligned} s_{11} &= 6EJ/l^3 & s_{44} &= 2EJ/l \\ s_{22} &= \sigma E/l & s_{55} &= \mu J/l \\ s_{33} &= 6EJ/l^3 & s_{66} &= 2EJ/l \\ s_{16} = s_{61} &= 3EJ/l^2 & s_{34} = s_{43} &= -3EJ/l^2 \end{aligned}\right\} \tag{5.6}$$

where E is Young's modulus, μ is the shear modulus, σ is the cross-sectional area, J is the polar second moment of area, and l is the shaft length; and it is noted that

$$2s_{16} - ls_{11} = 0, \qquad 2s_{34} + ls_{33} = 0 \tag{5.7}$$

For the truss

$$\left.\begin{aligned} s_{11} &= \frac{\sigma E}{l}[4\cos^2\beta_1 \sin\beta_1] \\ s_{22} &= \frac{\sigma E}{l}[4(1+\sin^3\beta_1+\sin^3\beta_3)] \\ s_{33} &= \frac{\sigma E}{l}[4\cos^2\beta_3 \sin\beta_3] \\ s_{44} &= \frac{\sigma E}{l}[4t_3^2(1+\sin^3\beta_1+\sin^3\beta_3)] \\ s_{55} &= \frac{\sigma E}{l}[4t_3^2\cos^2\beta_1 \sin\beta_1 + 4t_1^2\cos^2\beta_3 \sin\beta_3] \\ s_{66} &= \frac{\sigma E}{l}[4t_1^2(1+\sin^3\beta_1+\sin^3\beta_3)] \\ s_{16} = s_{61} &= \frac{\sigma E}{l}[4t_1 \sin^2\beta_1 \cos\beta_1] \\ s_{34} = s_{43} &= \frac{\sigma E}{l}[-4t_3 \sin^2\beta_3 \cos\beta_3] \end{aligned}\right\} \tag{5.8}$$

* Transverse shearing deformations are taken as small in comparison with bending deformations.

where E is Young's modulus, σ is the cross-section area of each member, l is the length of the truss, and β_1, β_3, t_1, and t_3 are as described in Fig. 11. The dimensions t_1 and t_3 are seen to be dependent upon β_1, β_3, and l through the following relationships:

$$t_1 = \frac{l}{2}\cot\beta_1, \qquad t_3 = \frac{l}{2}\cot\beta_3 \tag{5.9}$$

Equations (5.7) apply to the truss as well as to the shaft; and to verify that the restrictions contained in equation (4.15) are satisfied for both connections, note that

$$2S_{16} - LS_{11} \underset{(5.5)}{=} 2(-f_2 s_{11} + s_{16}) - Ls_{11} = 2s_{16} - (L+2f_2)s_{11} \tag{5.10}$$

where L is recalled to be the distance between P_0 and P_1 when the structure is in an undeformed state. But, as

$$l = L + 2f_2 \tag{5.11}$$

equations (5.7), (5.10), and (5.11) show that

$$2S_{16} - LS_{11} = 0$$

Similarly,

$$2S_{34} + LS_{33} \underset{(4.15,5.5)}{=} 2s_{34} + ls_{33} = 0.$$

Demonstration of elasticity effects

Consider now the elemental elastic system shown in Fig. 12, which consists of two solid homogeneous blocks connected by a *solid* circular shaft.

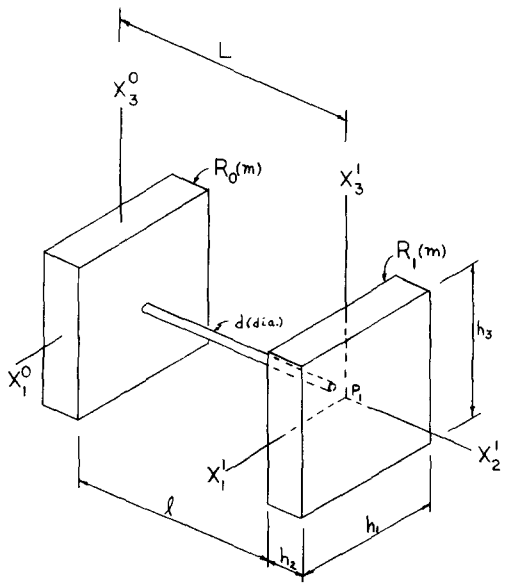

FIG. 12. Elemental elastic system.

To see how the motion and stability of this body are affected by the properties of the elastic shaft, take the following as the dimensions and elastic properties of the system (see Fig. 12 for h_1, h_2, h_3, d, and l):

$$\left.\begin{aligned} h_1 &= 10\text{ in.} & l &= 9\text{ in.} \\ h_2 &= 1\text{ in.} & d &= 0{\cdot}2\text{ in.} \\ h_3 &= 20\text{ in.} & E &= 10\times 10^6\text{ psi} \\ m &= 2\text{ slugs} & \mu &= 3{\cdot}8\times 10^6\text{ psi} \end{aligned}\right\} \tag{5.12}$$

Then

$$f_2 \underset{(5.1)}{=} -0{\cdot}5\text{ in.} \tag{5.13}$$

and

$$L \underset{(5.11)}{=} 10\text{ in.} \tag{5.14}$$

When the simple spin rate $\bar{\omega}$ (about an axis parallel to X_3^i) in reference frame N has the value

$$\bar{\omega} = \sqrt{(120\pi)}\text{ rad/sec} \tag{5.15}$$

the dimensionless parameters $\delta_1, \ldots, \delta_{10}$, as computed from equations (4.16), (5.5), (5.6), and (5.12)–(5.15) together with

$$\left.\begin{aligned} A &= \frac{m}{12}(h_2^2+h_3^2) \\ B &= \frac{m}{12}(h_1^2+h_3^2) \\ C &= \frac{m}{12}(h_1^2+h_2^2) \end{aligned}\right\} \tag{5.16}$$

are

$$\left.\begin{aligned} \delta_1 &= 0{\cdot}995 & \delta_6 &= 0{\cdot}206 \\ \delta_2 &= -0{\cdot}600 & \delta_7 &= 556 \\ \delta_3 &= 0{\cdot}196 & \delta_8 &= 0{\cdot}206 \\ \delta_4 &= 0{\cdot}0253 & \delta_9 &= 0{\cdot}616 \\ \delta_5 &= 0{\cdot}776 & \delta_{10} &= 2{\cdot}44 \end{aligned}\right\} \tag{5.17}$$

and the associated rigid body inertia parameters K_1 and K_2 are

$$K_1 \underset{(2.47,4.33)}{=} 0{\cdot}141, \qquad K_2 = -0{\cdot}600. \tag{5.18}$$

Figure 7 shows that the system is spinning about an axis of *minimum* moment of inertia of the associated rigid body. If the instability inequalities (4.22)–(4.30) are now applied, it appears that not one is satisfied; and, as system instability cannot be assured in this case, system stability is likely (although *not* guaranteed). To check on the stability status when the

body is in a circular orbit ($\varepsilon = 0$) of radius

$$R = 10{,}000 \text{ miles} \tag{5.19}$$

with an accompanying (constant) angular rate

$$n = \Omega \underset{(2.112)}{=} 3{\cdot}091 \times 10^{-4} \text{ rad/sec} \tag{5.20}$$

we now integrate* the equations of motion, noting that, as spin factor α has the large value

$$\alpha \underset{(3.1)}{=} \frac{\bar{\omega}}{\Omega} \underset{(5.15,5.20)}{=} 62{,}820 \tag{5.21}$$

it makes no difference whether the equations for torque-free motion, equations (2.87)–(2.95)′ and (2.96)–(2.98), or the complete equations (2.87)–(2.98) are employed for this purpose. Because a certain energy function, to be introduced later, is meaningful only in connection with the former set of equations, equations (2.87)′–(2.95)′ are used in preference to equations (2.87)–(2.95).

Consider the following initial conditions, which represent an initial disturbance:

$$\left.\begin{aligned}
&\omega_1/\bar{\omega} = 0{\cdot}002 \\
&\omega_2/\bar{\omega} = 0{\cdot}002 \\
&\omega_3/\bar{\omega} = 1{\cdot}000 \\
p_1/L = 0 \qquad &(p_1/L)' = 0 \\
p_2/L = 1/(2\delta_7 - 1) \qquad &(p_2/L)' = 0 \\
p_3/L = 0 \qquad &(p_3/L)' = 0 \\
\theta_1 = 4{\cdot}0 \times 10^{-4} \qquad &\theta_1' = 0 \\
\theta_2 = 4{\cdot}0 \times 10^{-4} \qquad &\theta_2' = 0 \\
\theta_3 = 4{\cdot}0 \times 10^{-4} \qquad &\theta_3' = 0 \\
\psi_1 = 0 \qquad \psi_2 = 0 \qquad &\psi_3 = 0
\end{aligned}\right\}. \tag{5.22}$$

As an alternative to presenting all the variables ψ_j, ω_j, p_j/L, and θ_j, the attitude of the system may be conveniently described in terms of an angle φ defined as

$$\begin{aligned}
\varphi &= \arccos(\mathbf{n}_3 \cdot \mathbf{c}_0) \\
&\underset{(2.2)}{=} \arccos(\cos\psi_1 \cos\psi_2)
\end{aligned} \tag{5.23}$$

φ is the angle between the body axis X_3^0 (fixed in R_0) and axis O_3, the normal to the orbit plane. The *elastic deformations* $(p_j/L, \theta_j)$ of the system are characterized, in part, by an energy function composed of the kinetic and potential (strain energy) energy of the system. (In the formation of the kinetic energy portion of this function, only linear and quadratic terms in p_j/L and θ_j are retained, as the governing equations were taken to be linear in these quantities. For the details of the energy function construction, see Appendix A.)

* Integration was performed on a Burroughs 5500 generously made available by the Stanford Computation Center.

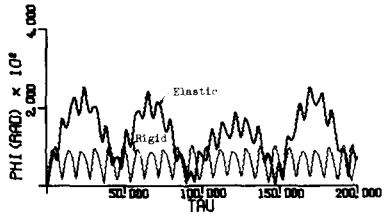

(a) Attitude Response

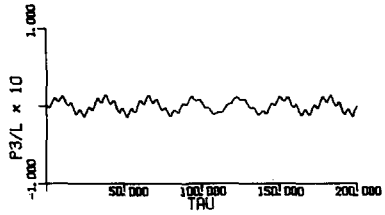

(b) Elastic Response

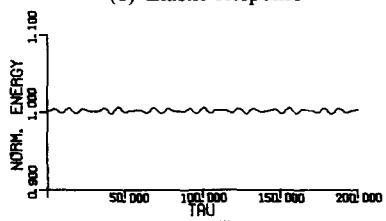

(c) Energy Function

FIG. 13. Stable elastic system with initial conditions (5.22).

In Fig. 13a, the value of φ, in radians, is plotted against τ both for the elastic system and for the associated rigid body. (The associated rigid body equations are given in Appendix B.) So that a meaningful comparison can be made between the attitude responses of the elastic system and the associated rigid body, the initial conditions for the latter are chosen to be

$$\left.\begin{aligned} \omega_1/\bar{\omega} &= 0{\cdot}002 \\ \omega_2/\bar{\omega} &= 0{\cdot}002 \\ \omega_3/\bar{\omega} &= 1{\cdot}000 \\ \psi_1 &= 0 \\ \psi_2 &= 0 \\ \psi_3 &= 0 \end{aligned}\right\} \tag{5.24}$$

these being compatible with the elastic system initial conditions in equation (5.22).

Figure 13a shows that the attitude response of the two systems is in striking contrast. The elasticity of the connection is seen to bring about attitude changes considerably in excess of those of the associated rigid body.

The elastic deformation p_3/L, which is typical, is displayed in Fig. 13b, and is seen to have an oscillatory character. Collectively, all elastic responses are represented by the aforementioned energy function, which, when normalized with respect to the associated rigid body energy [see equation (B7) in Appendix B], and then plotted against τ, as in Fig. 13c, turns out to be nearly constant. The associated rigid body energy is truly constant,

and thus permits the formation of a first integral of the rigid body equations of motion. In contrast, the variation in the normalized energy means that the energy function constructed in Appendix A does *not* lead to a first integral of the differential equations (2.87)′–(2.95)′, which is, however, not surprising, because these differential equations are valid only for small elastic deformations, i.e., they are, themselves, approximate relationships. The fluctuations in the energy function thus reflect the elastic character of the system, and they furnish an excellent means for determining the point in the integration at which the differential equations can no longer be regarded as describing real motions.

Suppose now that the initial disturbances are cut in half; that is, the initial values are taken to be

$$\left.\begin{aligned}
&\omega_1/\bar{\omega} = 0{\cdot}001 \\
&\omega_2/\bar{\omega} = 0{\cdot}001 \\
&\omega_3/\bar{\omega} = 1{\cdot}0000 \\
&p_1/L = 0 \qquad (p_1/L)' = 0 \\
&p_2/L = 1/(2\delta_7 - 1) \qquad (p_2/L)' = 0 \\
&p_3/L = 0 \qquad (p_3/L)' = 0 \\
&\theta_1 = 2{\cdot}0 \times 10^{-4} \qquad \theta_1' = 0 \\
&\theta_2 = 2{\cdot}0 \times 10^{-4} \qquad \theta_2' = 0 \\
&\theta_3 = 2{\cdot}0 \times 10^{-4} \qquad \theta_3' = 0 \\
&\psi_1 = 0 \qquad \psi_2 = 0 \qquad \psi_3 = 0
\end{aligned}\right\}. \tag{5.25}$$

This leads to the curves shown in Fig. 14, and a comparison of Figs. 13 and 14 shows that responses are correspondingly reduced. The system under consideration thus appears to be stable, as was expected on the basis of the stability analysis.

Suppose now that the values of h_1 and h_3 are changed to

$$h_1 = 20\,\text{in.} \quad \text{and} \quad h_3 = 10\,\text{in.} \tag{5.26}$$

which amounts to an interchange of the earlier values of h_1 and h_3. The δ parameters, obtained by reference to equations (4.16), (5.16), and (5.17), then become

$$\left.\begin{aligned}
&\delta_1 = 0{\cdot}980 \qquad \delta_6 = 0{\cdot}206 \\
&\delta_2 = 0{\cdot}600 \qquad \delta_7 = 556 \\
&\delta_3 = 0{\cdot}776 \qquad \delta_8 = 0{\cdot}206 \\
&\delta_4 = 0{\cdot}0253 \qquad \delta_9 = 2{\cdot}44 \\
&\delta_5 = 0{\cdot}196 \qquad \delta_{10} = 0{\cdot}616
\end{aligned}\right\} \tag{5.27}$$

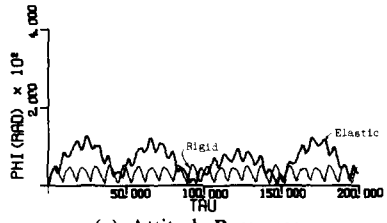

(a) Attitude Response

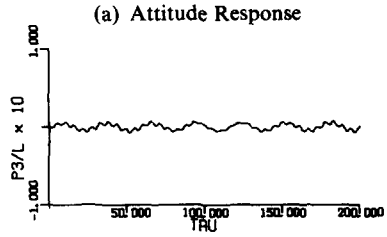

(b) Elastic Response

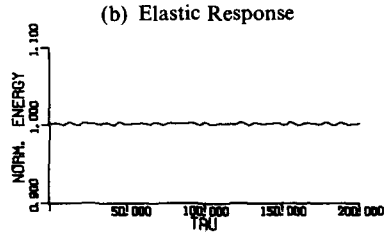

(c) Energy Function

FIG. 14. Stable elastic system with reduced initial conditions (5.25).

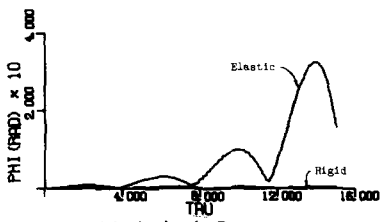

(a) Attitude Response

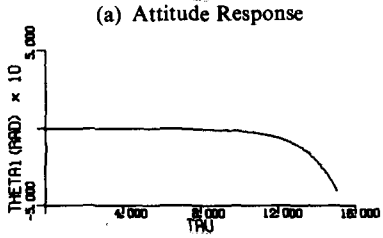

(b) Elastic Response

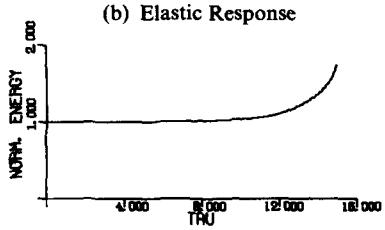

(c) Energy Function

FIG. 15. Unstable elastic system with initial conditions (5.22).

and the associated rigid body inertia parameters are

$$K_1 = -0{\cdot}501, \qquad K_2 = 0{\cdot}600 \tag{5.28}$$

which indicate that the associated rigid body spin axis is an axis of *maximum* moment of inertia. Application of inequalities (4.22)–(4.30) now shows that instability inequalities (4.22), (4.26), and (4.28) are satisfied; thus, instability is assured. The nature of the instability is illustrated by Fig. 15, which shows that the attitude angle φ continues to grow and that some of the elastic deformations, e.g., θ_1 as well as the normalized energy function, increase exponentially. Moreover, this instability appears before the system has made two complete revolutions ($\tau = 4\pi$) in reference frame N. These results confirm the prediction of instability, and further support is obtained from Fig. 16, which shows that a reduction of initial disturbances now cannot be used to obtain a reduction of response amplitudes, but merely delays the time at which a particular amplitude is attained.

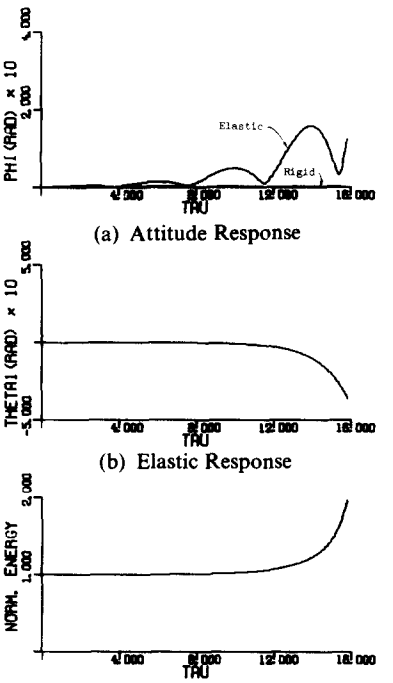

FIG. 16. Unstable elastic system with reduced initial conditions (5.25).

The importance of taking elasticity into account when trying to make a stability prediction is now apparent. On the basis of an analysis concerned solely with inertia properties, one would reach the wrong conclusions. In this connection it may be pointed out that a change in elastic properties can also have beneficial effects. For example, the unstable system just considered can be made not only stable, but "nearly rigid" by an increase in the shaft stiffness. If the diameter d of the shaft is increased from 0·2 in. to

$$d = 0{\cdot}4 \text{ in.} \tag{5.29}$$

the δ parameters become

$$\left.\begin{aligned} \delta_1 &= 0{\cdot}980 \qquad \delta_6 = 3{\cdot}290 \\ \delta_2 &= 0{\cdot}600 \qquad \delta_7 = 2220 \\ \delta_3 &= 12{\cdot}4 \qquad \delta_8 = 3{\cdot}29 \\ \delta_4 &= 0{\cdot}405 \qquad \delta_9 = 39{\cdot}1 \\ \delta_5 &= 3{\cdot}13 \qquad \delta_{10} = 9{\cdot}85 \end{aligned}\right\} \tag{5.30}$$

and a check of the instability inequalities shows that none comes close to being satisfied. Hence, stability is expected, and with the initial conditions used previously [see (5.22) and (5.24)], integration of the full equations of motion leads to Fig. 17. The values of φ for the elastic body and for the associated rigid body are now nearly identical and the normalized energy remains essentially constant, which shows that the values of p_j/L and θ_j remain small. The elastic system is thus seen to be moving like a rigid body.

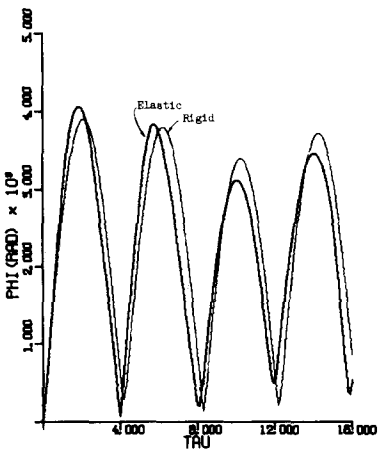

(a) Attitude Response

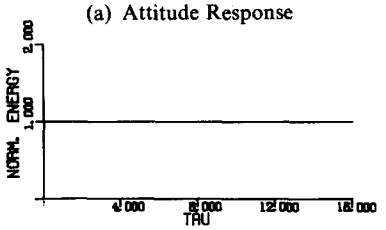

(b) Energy Function

FIG. 17. Nearly rigid behavior.

Types of instability

In view of the complex character and large number of the instability inequalities (4.22)–(4.30), it is gratifying that one can identify at least two clear-cut types of unstable behavior. The first of these, called "attitude instability," may be said to be obtained when, subsequent to any disturbance, elastic deformations remain small, whereas the motion of each end

body differs markedly from simple spin; and the second type, called "deformation instability," is characterized by rapidly growing elastic deformations, but relatively minor differences between the motions of the end bodies prior and subsequent to a disturbance. Consider, for example, the system described by equations (5.12), but change the shaft length and diameter to

$$l = 14 \text{ in.}, \qquad d = 0{\cdot}50 \text{ in.} \tag{5.31}$$

Then the δ's have the values

$$\left.\begin{aligned} \delta_1 &= 0{\cdot}995 & \delta_6 &= 2{\cdot}14 \\ \delta_2 &= -0{\cdot}600 & \delta_7 &= 2230 \\ \delta_3 &= 4{\cdot}64 & \delta_8 &= 2{\cdot}14 \\ \delta_4 &= 0{\cdot}636 & \delta_9 &= 14{\cdot}4 \\ \delta_5 &= 18{\cdot}4 & \delta_{10} &= 57{\cdot}1 \end{aligned}\right\} \tag{5.32}$$

and the associated rigid body inertia parameters are

$$K_1 = -0{\cdot}257 \qquad K_2 = -0{\cdot}600. \tag{5.33}$$

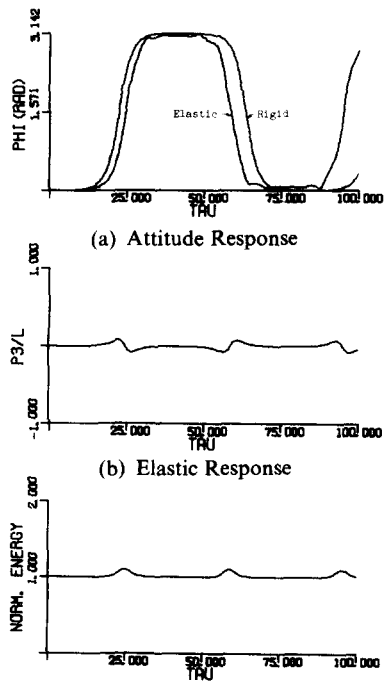

(a) Attitude Response

(b) Elastic Response

(c) Energy Function

FIG. 18. Attitude instability with initial conditions (5.25).

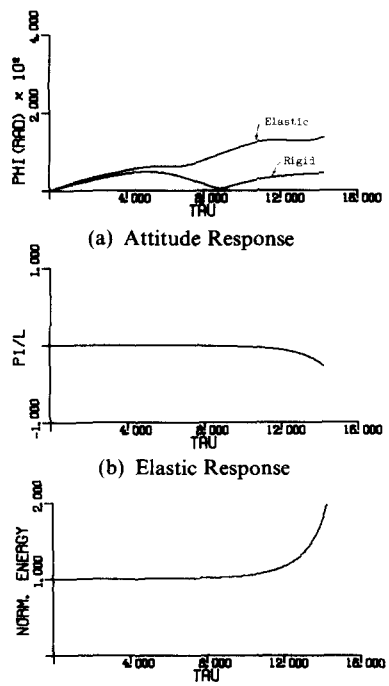

(a) Attitude Response

(b) Elastic Response

(c) Energy Function

FIG. 19. Deformation instability with initial conditions (5.25).

The associated rigid body is now spinning about an axis of *intermediate* moment of inertia; a check of the instability inequalities (4.22)–(4.30) reveals that one, namely (4.25), is satisfied; and the plots shown in Fig. 18 indicate that the attitude angle φ (see Fig. 18a) grows rapidly to the large value π, but that both the elastic deformation p_3/L (see Fig. 18b) and the energy function (see Fig. 18c) fluctuate only moderately. Furthermore, Fig. 18a suggests that the motion of the entire system resembles that of the associated rigid body. Hence we have a typical case of "attitude instability." Next, if l and d are changed to

$$l = 9 \text{ in.}, \qquad d = 0{\cdot}16 \text{ in.} \tag{5.34}$$

then the δ parameters become

$$\left.\begin{aligned} \delta_1 &= 0{\cdot}995 & \delta_6 &= 0{\cdot}0843 \\ \delta_2 &= -0{\cdot}600 & \delta_7 &= 356 \\ \delta_3 &= 0{\cdot}0801 & \delta_8 &= 0{\cdot}0843 \\ \delta_4 &= 0{\cdot}0104 & \delta_9 &= 0{\cdot}252 \\ \delta_5 &= 0{\cdot}318 & \delta_{10} &= 1{\cdot}00 \end{aligned}\right\} \tag{5.35}$$

and

$$K_1 = 0{\cdot}141, \qquad K_2 = -0{\cdot}600. \tag{5.36}$$

The instability inequality (4.22) is now satisfied, and integration with initial conditions (5.25) leads to Fig. 19, which shows that the value of the attitude angle φ changes very slowly while the elastic deformation p_1/L grows rapidly and the energy function fails to remain even nearly constant. This is what is meant by "deformation instability."

Space station

The model considered for the remaining examples is intended to have properties appropriate for a rotating space station. Such parameters as spin rate and dimensions are selected on the basis of information contained in [1];* e.g., the distance between the end bodies is taken greater than 100 ft, and the angular rate ($\bar{\omega}$) of the station is kept below 4 rev/min.

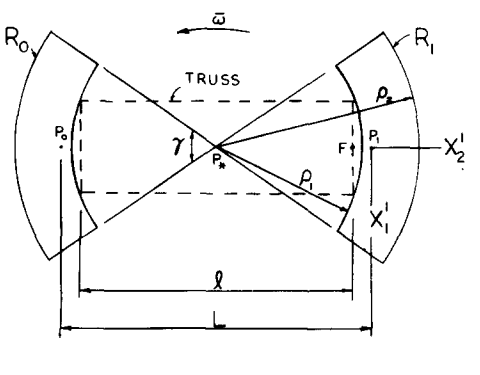

FIG. 20. Space station.

* Numbers in brackets designate references listed at the end of the first part of this paper.

Figure 20 shows a plan view of the model. As a matter of convenience, R_0 and R_1 may be regarded as solid homogeneous bodies of mass density w, and the mass m of each is then given by

$$m = w\frac{\gamma}{2}(\rho_2^2 - \rho_1^2)h_3 \tag{5.37}$$

where the angle γ and the radial distances ρ_1 and ρ_2 are shown in Fig. 20. The principal centroidal moments of inertia for R_i are

$$\left.\begin{aligned} A &= m\left[\left(\frac{\rho_1^2+\rho_2^2}{4}\right)\left(1+\frac{\sin\gamma}{\gamma}\right)+\frac{h_3^2}{12}-\frac{L^2}{4}\right] \\ B &= m\left[\left(\frac{\rho_1^2+\rho_2^2}{4}\right)\left(1-\frac{\sin\gamma}{\gamma}\right)+\frac{h_3^2}{12}\right] \\ C &= m\left[\frac{\rho_1^2+\rho_2^2}{2}-\frac{L^2}{4}\right] \end{aligned}\right\} \tag{5.38}$$

where L, the distance between P_0 and P_1, is given by

$$L = \frac{8}{3}\frac{\sin\gamma/2}{\gamma}\left[\frac{\rho_1^2+\rho_1\rho_2+\rho_2^2}{\rho_1+\rho_2}\right] \tag{5.39}$$

and where h_3 is the height of the cylindrical sections shown in Fig. 20. R_0 and R_1 are connected by the twelve member truss shown in Fig. 11. The length l of the structure, found by reference to Figs. 11 and 20, is

$$l = 2\sqrt{(\rho_1^2 - t_1^2)}. \tag{5.40}$$

Gravitational effects

In order to substantiate the claim made previously that gravitational forces have negligible effects when the spin factor α is high, we consider the space station in a circular orbit, first leaving gravitational effects out of account, i.e., omitting gravitational terms from equations (2.87)–(2.95), and the repeating the calculations with the *complete* set of equations.

As before, we specify a circular orbit with

$$\begin{aligned} R &= 10{,}000 \text{ miles} \\ \Omega &= 3{\cdot}091 \times 10^{-4} \text{ rad/sec.} \end{aligned} \tag{5.41}$$

The space station is described as follows (see Fig. 20):

$$\left.\begin{aligned} \rho_1 &= 90 \text{ ft} \\ \rho_2 &= 100 \text{ ft} \\ h_3 &= 25 \text{ ft} \\ \gamma &= \pi/4 \text{ rad} \\ w &= 10/32{\cdot}2 \text{ slugs/ft}^3 \end{aligned}\right\} \tag{5.42}$$

and (see Fig. 20)

$$\left.\begin{aligned} \sigma &= 0{\cdot}25\ \text{in}^2 \\ E &= 10\times 10^6\ \text{psi} \\ t_1 &= 5{\cdot}0\ \text{ft} \\ t_3 &= 4{\cdot}0\ \text{ft} \end{aligned}\right\}. \tag{5.43}$$

Then, from equations (5.37)–(5.40),

$$\left.\begin{aligned} m &= 5790\ \text{slugs} \\ A/m &= 64{\cdot}67\ \text{ft}^2 \\ B/m &= 503{\cdot}2\ \text{ft}^2 \\ C/m &= 463{\cdot}7\ \text{ft}^2 \\ L &= 185{\cdot}3\ \text{ft} \\ l &= 179{\cdot}7\ \text{ft} \end{aligned}\right\} \tag{5.44}$$

while, from equation (5.11),

$$f_2 = -2{\cdot}80\ \text{ft}. \tag{5.45}$$

Finally, from equation (5.9), the truss angles β_1 and β_3 are

$$\beta_1 = 1{\cdot}515\ \text{rad}, \qquad \beta_3 = 1{\cdot}526\ \text{rad}. \tag{5.46}$$

An angular rate (in reference frame N) of 3 rev/min corresponds to

$$\bar{\omega} = \frac{\pi}{10}\ \text{rad/sec} \tag{5.47}$$

and it may be noted that this provides at a radius of 100 ft an "artificial gravity" of $\pi^2\ \text{ft sec}^{-2}$, or approximately three-tenths (0.3) of the gravitational acceleration at the surface of the earth.

The spin factor α is given by

$$\alpha \underset{(3.1)}{=} \frac{\bar{\omega}}{\Omega} \underset{(5.41,5.47)}{=} 1016{\cdot}45 \tag{5.48}$$

and $\delta_1, \ldots, \delta_{10}$, found by using equations (4.16), (5.5), (5.8), and (5.41)–(5.47), have the values

$$\left.\begin{aligned} \delta_1 &= 0{\cdot}611 & \delta_6 &= 0{\cdot}300 \\ \delta_2 &= 0{\cdot}793 & \delta_7 &= 291 \\ \delta_3 &= 73{\cdot}6 & \delta_8 &= 0{\cdot}192 \\ \delta_4 &= 0{\cdot}0191 & \delta_9 &= 102 \\ \delta_5 &= 16{\cdot}0 & \delta_{10} &= 22{\cdot}2 \end{aligned}\right\}. \tag{5.49}$$

The associated rigid body inertia parameters are given by

$$K_1 \underset{(2.47,4.33)}{=} -0{\cdot}988, \qquad K_2 = 0{\cdot}793 \tag{5.50}$$

so that the associated rigid body is spinning about an axis of *maximum* moment of inertia. (Note that the axis X_3^i is an axis of *intermediate* centroidal principal moment of inertia of R_i, as indicated by the positive values of δ_1 and δ_2.)

When each of the instability inequalities (4.22)–(4.30) is checked, it appears that none is satisfied; hence, stability is suggested.

A numerical integration of the full, nonlinear equations (2.87)′–(2.95)′ and (2.96)–(2.98) is now carried out with the following initial conditions (which describe an initial disturbance of R_0):

$$\left.\begin{array}{llll} \omega_1/\bar{\omega} = 0{\cdot}01 & & & \\ \omega_2/\bar{\omega} = 0{\cdot}01 & & & \\ \omega_3/\bar{\omega} = 1{\cdot}01 & & & \\ p_1/L = 0 & & (p_1/L)' = 0 & \\ p_2/L = 1/(2\delta_7 - 1) & & (p_2/L)' = 0 & \\ p_3/L = 0 & & (p_3/L)' = 0 & \\ \theta_1 = 0 & & \theta_1' = -0{\cdot}01 & \\ \theta_2 = 0 & & \theta_2' = -0{\cdot}01 & \\ \theta_3 = 0 & & \theta_3' = -0{\cdot}01 & \\ \psi_1 = 0 & \psi_2 = 0 & \psi_3 = 0 & \end{array}\right\} . \tag{5.51}$$

The three plots shown in Fig. 21 characterize the results of this integration. The first, Fig. 21a, reveals an oscillatory variation of the angle φ between the body-fixed axis X_3^0 and the orbit plane normal (with which X_3^0 coincides initially), and R_0 is thus seen to be performing a "nutational" motion. The deformation p_1/L, plotted in Fig. 21b, is representative of all of the elastic variables, and thus shows that vibrations of the elastic system accompany the aforementioned nutation. The behavior both of φ and of the elastic variables is thus compatible with the designation "stable" for the undisturbed motion, and the fact the energy function remains very nearly constant, as indicated in Fig. 21c, is yet another indication of stability. Finally, when the integration is repeated subsequent to a reduction of all initial disturbances, the response is found to be simply a reduced version of the earlier response. One may, therefore, conclude that the instability inequalities lead to a correct conjecture in the present case.

When the integration results described in Fig. 21 are compared with the corresponding results obtained by using equations (2.87)–(2.95) in place of equations (2.87)′–(2.95)′, it becomes clear that the relative importance of gravitational effects for structures of the kind under consideration is negligible. Figure 22 shows the results of such an integration, and it can be seen that there is no discernible difference between the curves shown there and their counterparts in Fig. 21. This outcome agrees with the conclusions reached in Section 3, because the spin factor α has the value 1016·45 and thus falls into the "high" range.

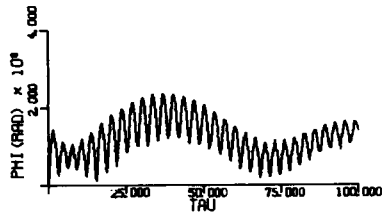

(a) Attitude Response

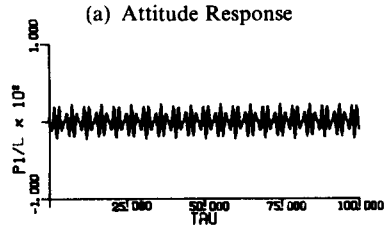

(b) Elastic Response

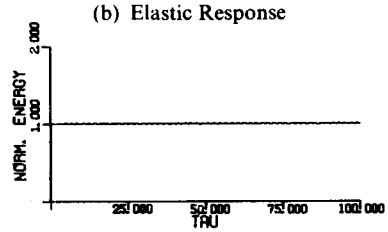

(c) Energy Function

FIG. 21. Vehicle in circular orbit *without* effects of gravity.

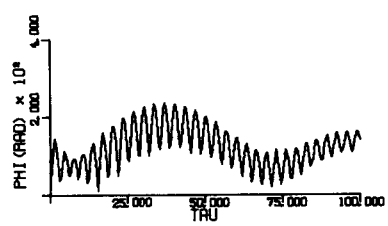

(a) Attitude Response

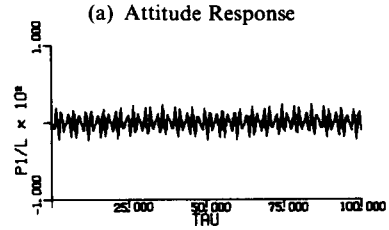

(b) Elastic Response

FIG. 22. Vehicle in circular orbit *with* effects of gravity.

Sensitivity to parameter values

If the values of t_1 and t_3 (see Fig. 11) are changed from those given in equation (5.43) to

$$t_1 = t_3 = 1 \text{ ft} \tag{5.52}$$

the values of l, f_2, β_1, and β_3 become

$$l = 180{\cdot}0\,\text{ft}, \qquad f_2 = -2{\cdot}67\,\text{ft}, \qquad \beta_1 = \beta_3 = 1{\cdot}560\,\text{rad} \tag{5.53}$$

and $\delta_1, \ldots, \delta_{10}$ are changed to

$$\left.\begin{aligned} \delta_1 &= 0{\cdot}611 & \delta_6 &= 0{\cdot}0120 \\ \delta_2 &= 0{\cdot}793 & \delta_7 &= 291 \\ \delta_3 &= 4{\cdot}60 & \delta_8 &= 0{\cdot}0120 \\ \delta_4 &= 0{\cdot}0000477 & \delta_9 &= 6{\cdot}37 \\ \delta_5 &= 0{\cdot}641 & \delta_{10} &= 0{\cdot}889 \end{aligned}\right\} \tag{5.54}$$

The inequalities (4.22) and (4.26) are now satisfied; instability is thus assured; and integration with the initial conditions (5.51) leads to the curves shown in Fig. 23, in which instability manifests itself in three distinct ways. The attitude angle φ grows, the elastic deformation

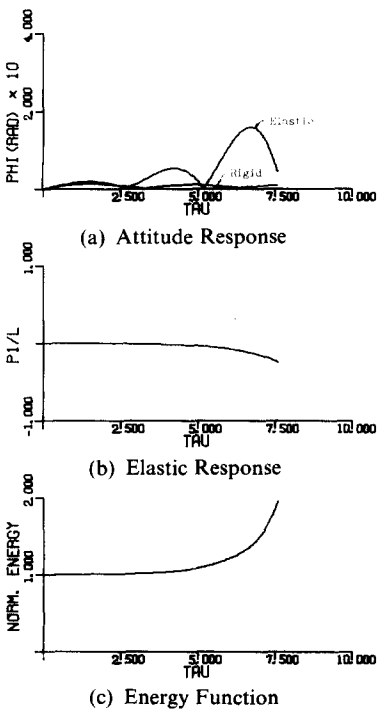

FIG. 23. Instability caused by a change in truss dimensions.

p_1/L increases exponentially, and the energy function does not remain even approximately constant. This instability manifests itself before the vehicle has made even one revolution (i.e., $\tau = 2\pi$). As the present example differs from the one described in Fig. 21 only because it involves different values of the truss dimensions $t_1, t_3, l, \beta_1, \beta_3$, and f_2, it is evident that the properties of the elastic connection have an important bearing on vehicle stability.

By using the instability inequalities, it can also be verified that stability is intimately related to the value of the angle γ (see Fig. 20) and that even the value of $\bar{\omega}$ may be critical. For example, for the system described by equations (5.42)–(5.46), $\bar{\omega}$ has the critical value

$$\bar{\omega}_c \approx 1{\cdot}11 \text{ rad/sec} \tag{5.55}$$

as the instability inequality (4.26) is satisfied whenever $\bar{\omega}$ equals or exceeds $\bar{\omega}_c$. This fact is of interest for the following reason. As it has been demonstrated previously that a high spin factor α reduces the importance of gravitational effects, one might, therefore, be tempted to generate a high α by means of a high $\bar{\omega}$. But it is now clear that this may not be advisable, because high values of $\bar{\omega}$ can, themselves, lead to instability.

CONCLUSION

In Part I of this paper the equations of motion were derived for a rotating satellite composed to two elastically connected, inertially identical, unsymmetrical rigid bodies. Part II contained a stability analysis in which "instability inequalities" were formulated by reference to the differential equations of motion. A procedure for the application of these inequalities, which are expressed in terms of dimensionless parameters reflecting the inertia and the elastic properties as well as the spin rate of the vehicle, was also outlined. In Part III the effect of elasticity on vehicle motion is demonstrated, and various types of instabilities are illustrated.

The principal conclusion reached in this investigation is that the nature of the elastic connection can appreciably affect the stability of the vehicle. Specifically, certain vehicle configurations which are predicted to be stable when analyzed as if rigid must be classed as unstable when flexibility is taken into account. Furthermore, as vehicle stability can be sensitive to dimension and spin rate changes, vehicle parameters should be selected with considerable care if instabilities are to be avoided.

(*Received* 4 *February* 1966; *revised* 10 *October* 1966)

APPENDIX A

ELASTIC SYSTEM ENERGY FUNCTION

In order to be consistent with the formulation of the equations of motion [equations (2.87)′–(2.95)′], which are nonlinear in ω_j and linear in p_j and θ_j, one must construct the energy function E so that it contains all second and lower degree terms in p_j and θ_j. In general terms, E is given by

$$E = \sum_{i=0}^{1} {}^{N}K^{R_i/P_*} + P \tag{A1}$$

where ${}^{N}K^{R_i/P^*}$ is the kinetic energy in N of body R_i with respect to P_*, and P is the potential energy (strain energy) of the deformed elastic connecting structure. Moreover,

$${}^{N}K^{R_i/P_*} = {}^{N}K^{P_i/P_*} + {}^{N}K^{R_i/P_i} \tag{A2}$$

where

$$^{N}K^{P_i/P_*} = \tfrac{1}{2}m(^{N}\mathbf{v}^{P_i/P_*})^2 \tag{A3}$$

and

$$^{N}K^{R_i/P_i} = \tfrac{1}{2}{}^{N}\boldsymbol{\omega}^{R_i} \cdot \mathbf{I}_i \cdot {}^{N}\boldsymbol{\omega}^{R_i} \tag{A4}$$

From equations (2.6), (2.11), and (A3)

$$\begin{aligned} ^{N}K^{P_0/P_*} &= {}^{N}K^{P_1/P_*} \\ &= \frac{m}{8}\{[\dot{p}_1 + \omega_2 p_3 - \omega_3(L+p_2)]^2 + [\dot{p}_2 + \omega_3 p_1 - \omega_1 p_3]^2 \\ &\quad + [\dot{p}_3 + \omega_1(L+p_2) - \omega_2 p_1]^2\} \end{aligned} \tag{A5}$$

and from equations (A4), (2.16), and (2.6),

$$^{N}K^{R_0/P_0} = \tfrac{1}{2}[A\omega_1^2 + B\omega_2^2 + C\omega_3^2]. \tag{A6}$$

Next, $^{N}K^{R_1/P_1}$ is formed by using a version of $^{N}\omega^{R_1}$ which contains all quadratic terms in θ_j so that, after normalization with (2.86), the kinetic energy of the elastic system with respect to P_* is seen to be

$$\begin{aligned} \sum_{i=0}^{1} {}^{N}K^{R_i/P_*} \underset{(A2,A5,A6)}{=\!=} & \left(\frac{mL^2}{2}\bar{\omega}^2\right)\left\{\frac{1}{2}\left[\frac{p_1'}{L} + \frac{\omega_2}{\bar{\omega}}\frac{p_3}{L} - \frac{\omega_3}{\bar{\omega}}\left(1+\frac{p_2}{L}\right)\right]^2\right. \\ & + \frac{1}{2}\left[\frac{p_2'}{L} + \frac{\omega_3}{\bar{\omega}}\frac{p_1}{L} - \frac{\omega_1}{\bar{\omega}}\frac{p_3}{L}\right]^2 + \frac{1}{2}\left[\frac{p_3'}{L} + \frac{\omega_1}{\bar{\omega}}\left(1+\frac{p_2}{L}\right) - \frac{\omega_2}{\bar{\omega}}\frac{p_1}{L}\right]^2 \\ & + \frac{A}{mL^2}\frac{\omega_1^2}{\bar{\omega}^2} + \frac{B}{mL^2}\frac{\omega_2^2}{\bar{\omega}^2} + \frac{C}{mL^2}\frac{\omega_3^2}{\bar{\omega}} \\ & + \frac{A}{mL^2}\left[\theta_1' + \frac{\omega_1}{\bar{\omega}}\left(1 - \frac{\theta_2^2}{2} - \frac{\theta_3^2}{2}\right) + \frac{\omega_2}{\bar{\omega}}(\theta_3 + \theta_1\theta_2) - \frac{\omega_3}{\bar{\omega}}(\theta_2 - \theta_1\theta_3) + \theta_2'\theta_3\right]^2 \\ & + \frac{B}{mL^2}\left[\theta_2' + \frac{\omega_2}{\bar{\omega}}\left(1 - \frac{\theta_3^2}{2} - \frac{\theta_1^2}{2}\right) + \frac{\omega_3}{\bar{\omega}}(\theta_1 + \theta_2\theta_3) - \frac{\omega_1}{\bar{\omega}}\theta_3 - \theta_1'\theta_3\right]^2 \\ & \left. + \frac{C}{mL^2}\left[\theta_3' + \frac{\omega_3}{\bar{\omega}}\left(1 - \frac{\theta_1^2}{2} - \frac{\theta_2^2}{2}\right) + \frac{\omega_1}{\bar{\omega}}\theta_2 - \frac{\omega_2}{\bar{\omega}}\theta_1 + \theta_1'\theta_2\right]^2\right\} \end{aligned} \tag{A7}$$

where

$$\begin{aligned} &\frac{A}{mL^2} \underset{(4.16)}{=\!=} \frac{\delta_8}{\delta_9} \\ &\frac{B}{mL^2} \underset{(4.16)}{=\!=} \left(\frac{\delta_6}{\delta_{10}} - \frac{\delta_8}{\delta_9}\right)\frac{1}{\delta_2} \\ &\frac{C}{mL^2} \underset{(4.16)}{=\!=} \frac{\delta_6}{\delta_{10}}. \end{aligned} \tag{A8}$$

The potential energy (strain energy) of the deformed structure may be expressed as (see Gere and Weaver [18], p. 35)

$$P = \tfrac{1}{2}\{x\}^T[S]\{x\} \tag{A9}$$

where $\{x\}^T$ is the transpose of the column matrix in equation (2.30). Using the δ parameters and the structural limitations that were specified in Section 4, one may express P as

$$P \underset{(A8,4.16)}{=} \left(\frac{mL^2\bar{\omega}^2}{2}\right)\left[\delta_6\left(\frac{p_1}{2}\right)^2+\delta_7\left(\frac{p_2}{L}\right)^2+\delta_8\left(\frac{p_3}{L}\right)^2+\frac{\delta_8}{\delta_9}\delta_3\theta_1^2 + \left(\frac{\delta_6}{\delta_{10}}-\frac{\delta_8}{\delta_9}\right)\frac{\delta_4}{\delta_2}\theta_2^2+\frac{\delta_6}{\delta_{10}}\delta_5\theta_3^2+\delta_6\frac{p_1}{L}\theta_3-\delta_8\frac{p_3}{L}\theta_1\right] \tag{A10}$$

The energy function E may now be obtained by substituting from equations (A7), (A8), and (A10) into equation (A1).

APPENDIX B

ASSOCIATED RIGID BODY EQUATIONS OF MOTION AND FIRST INTEGRAL

The normalized differential equations of motion for the associated rigid body in a torque-free state are

$$\frac{\omega_1'}{\bar{\omega}} = K_1\frac{\omega_2}{\bar{\omega}}\frac{\omega_3}{\bar{\omega}} \tag{B1}$$

$$\frac{\omega_2'}{\bar{\omega}} = K_2\frac{\omega_3}{\bar{\omega}}\frac{\omega_1}{\bar{\omega}} \tag{B2}$$

$$\frac{\omega_3'}{\bar{\omega}} = K_3\frac{\omega_1}{\bar{\omega}}\frac{\omega_2}{\bar{\omega}} = -\frac{(K_1+K_2)}{(1+K_1K_2)}\frac{\omega_1}{\bar{\omega}}\frac{\omega_2}{\bar{\omega}} \tag{B3}$$

together with equations (2.96)–(2.98).

One first integral of the equations (B1)–(B3) is

$$\Phi_* = \frac{1+K_3}{1-K_1}\left(\frac{\omega_1}{\bar{\omega}}\right)^2+\frac{1-K_3}{1+K_2}\left(\frac{\omega_2}{\bar{\omega}}\right)^2+\left(\frac{\omega_3}{\bar{\omega}}\right)^2 \tag{B4}$$

where

$$K_3 = -\frac{(K_1+K_2)}{(1+K_1K_2)} \tag{B5}$$

and Φ_* is a constant. The kinetic (and hence total) energy in N of R_* with respect to P_* is given by

$${}^NK^{R_*/P_*} = \tfrac{1}{2}{}^N\boldsymbol{\omega}^{R_*}\cdot\mathbf{I}_*\cdot{}^N\boldsymbol{\omega}^{R_*} \tag{B6}$$

and may be expressed in terms of Φ_* as

$${}^NK^{R_*/P_*} = (\tfrac{1}{2}I_3\bar{\omega}^2)\Phi_* \tag{B7}$$